Journal of Asian Concrete Federation
Vol. 11, No. 4, pp. 33-44, December 2025
ISSN 2465-7964/ eISSN 2465-7972
DOI http://dx.doi.org/10.18702/acf.2025.11.4.33

Technical Paper

Application of alginate–based epoxy microcapsule in self–healing concrete

Danyang Zhao, Jia–ao Hou, Yishuang Zhang, Yu Li, Cheuk Lun Chow*, Denvid Lau*

(Received: 30-Oct-2025; Revised: 23-Nov-2025; Accepted: 07-Dec-2025; Published online: 27-Dec-2025)

Abstract: During the service life of concrete structures, microcracks are prone to occur, leading to strength degradation and reduced durability. Traditional repair methods rely on manual intervention and are unable to promptly detect and repair cracks. In this study, a novel alginate-based microcapsule was developed, consisting of calcium alginate as the shell and epoxy as the core, to enable autonomous crack healing in concrete. This system allows the capsules to rupture upon crack formation and release the core material to initiate the healing reaction. Experimental results demonstrated that microcapsules possessed a spherical morphology and excellent thermal stability. The core content reached 84.39% before immersion and remained at 72.12% after 1 day in cement filtrate, indicating outstanding core retention capacity. Mortar specimens containing 5 wt% microcapsules achieved a compressive strength recovery rate of up to 145.4% after 7 days of self-healing, as the ruptured microcapsules released epoxy and formed dense interfacial networks within crack regions. Molecular dynamics simulation was employed to investigate the reaction process between epoxy and curing agent, revealing the stepwise network formation during crosslinking. The results confirmed the feasibility and remarkable self-healing performance of the alginate-based epoxy microcapsule system, providing a sustainable and cost-effective approach to enhancing structural durability.

Keywords: Self-healing concrete; Epoxy microcapsule; Calcium alginate; Molecular dynamics simulation

1. Introduction

Concrete structures inevitably develop cracks during their service life, which provide channels for harmful substances such as chloride ions, carbon dioxide, and moisture to penetrate into the interior of the material, thereby significantly accelerating the corrosion of reinforcing steel [1-5]. Meanwhile, the presence of cracks aggravates other deterioration processes, including freeze-thaw damage, alkali-aggregate reaction, and sulfate attack, further reducing structural durability. The long-term propagation of cracks not only shortens the service life of structures but also substantially increases maintenance and strengthening costs, imposing adverse effects on structural safety and sustainability.

Traditional crack repair methods for concrete mainly include grouting, injection, and surface patching techniques [6]. These approaches typically rely on manual operations, in which externally applied repair materials are used to seal or fill cracks, thereby preventing the further ingress of harmful substances. Although such methods can temporarily restore the compactness and partial mechanical integrity of

*Corresponding author **Cheuk Lun Chow,** *Department of Architecture and Civil Engineering, City University of Hong Kong. E–mail: cheuchow@cityu.edu.hk*
*Corresponding author **Denvid Lau,** *Department of Architecture and Civil Engineering, City University of Hong Kong. E–mail: denvid.lau@cityu.edu.hk*
Danyang Zhao, *Department of Architecture and Civil Engineering, City University of Hong Kong. E–mail: dyzhao6–c@my.cityu.edu.hk*
Jia–ao Hou, *Department of Architecture and Civil Engineering, City University of Hong Kong. E–mail: jahou2–c@my.cityu.edu.hk*
Yishuang Zhang, *Department of Architecture and Civil Engineering, City University of Hong Kong. E–mail: yiszhang2–c@my.cityu.edu.hk*
Yu Li, *Department of Architecture and Civil Engineering, City University of Hong Kong. E–mail: yuli239–c@my.cityu.edu.hk*

concrete, they are often labor-intensive and time-consuming under long-term service conditions. In addition, it is difficult to detect and repair internal cracks and the effectiveness of repair is highly influenced by environmental conditions. Furthermore, traditional methods are essentially passive, requiring human intervention only after crack formation. Consequently, they cannot achieve real-time self-sensing and autonomous repair of structures, making them inadequate to meet the modern demands of infrastructure for long service life, low maintenance, and sustainability [7].

In recent years, self-healing concrete technology has attracted widespread attention as an innovative solution for enhancing structural durability. Among various approaches, microcapsule-based self-healing systems are regarded as one of the most promising strategies [8]. In this technique, healing agents are encapsulated within a protective shell, and when cracks occur or external stress is applied, the capsules rupture, releasing the core healing agent. The released agent reacts with external moisture or curing agents to form new solid products, thereby autonomously filling and sealing the cracks. Compared with traditional repair methods, the microcapsule-based self-healing system offers remarkable advantages such as automatic activation, independence from external intervention, adaptability to complex environments, and the potential for multiple healing cycles [6, 9]. These merits not only significantly enhance the long-term durability of concrete structures but also provide new insights for the development of green and intelligent construction materials. Calcium alginate (CA) was one of the good candidates as microcapsule shell material due to its excellent biocompatibility and environmental friendliness, which facilitates safe incorporation into cementitious systems [10]. Its porous gel-like network provides superior encapsulation capability, enabling effective storage of the epoxy core material. In addition, CA exhibits good water resistance and moderate mechanical stability, which ensure survivability during mixing and service conditions. Notably, CA possesses intrinsic swelling behavior upon contact with moisture, contributing to rapid crack sealing in the early stage, while the epoxy core subsequently undergoes crosslinking and curing to achieve long-term healing.

Based on the above research background, a green microcapsule system with CA as the shell and epoxy as the core was proposed for the self-healing of concrete. The microcapsules were prepared via an ionic crosslinking method, resulting in a structurally stable and well-encapsulated morphology. The morphological characteristics, particle size distribution, chemical structure, and thermal stability were systematically analyzed. Furthermore, the prepared microcapsules were incorporated into mortar to evaluate their survivability and healing performance during mixing, water addition, and curing processes. Molecular dynamics (MD) simulation was employed to investigate the crosslinking and curing mechanism of the core healing agent at the crack interface. The results demonstrated that the proposed microcapsules exhibit excellent environmental compatibility and durability, effectively enhancing the mechanical strength of concrete after self-healing. This study provides theoretical support for the development of intelligent self-healing concrete technologies based on polymer materials.

2. Material and method

2.1 Materials

The cement used in this study was ordinary Portland cement (P.O. 42.5), supplied by Tianshan Cement Co., Ltd. Standard sand was obtained from Xiamen ISO Standard Sand Co., Ltd. The epoxy was of type E-51 (WSR618, Phoenix Materials Co., Ltd.), and the curing agent was 2-methylimidazole (2-MI, Macklin Biochemical Co., Ltd., Shanghai). Sodium alginate and anhydrous calcium chloride, both purchased from Macklin Biochemical Co., Ltd., Shanghai, were used to construct the microcapsule shell. All chemicals were used as received without further purification. Deionized water was used throughout the experiments.

2.2 Encapsulation of microcapsule

CA-epoxy microcapsules were prepared via an ionic crosslinking method. A 1.5 wt% sodium alginate (SA) solution was mechanically mixed with epoxy at a mass ratio of 5:1 (epoxy to SA) to form a homogeneous

mixture. Specific content and concentration of used raw materials are shown in Table 1. The mixture was stirred at a constant speed of 600 rpm using a mechanical mixer to ensure uniform dispersion of epoxy within the SA solution. The resulting mixture was then dripped through a needle into a 2 wt% calcium chloride ($CaCl_2$) solution, allowing Ca^{2+} ions to crosslink with the sodium alginate molecular chains for 30 min, thereby forming a stable CA gel network. The obtained microcapsules were subsequently filtered, washed with deionized water, and dried at 30 °C. The dried microcapsules were collected and sealed for subsequent use.

Table 1 Materials used for microcapsule encapsulation.

Material	Content/Concentration
Sodium alginate (SA)	3 g
E51 Epoxy	15 g
Calcium chloride ($CaCl_2$) solution	2 wt%

2.3. Mortar specimen preparation

Mortar was prepared with a mass ratio of cement : sand : water = 1 : 3 : 0.5. The microcapsule dosages were set at 0%, 1%, 3%, 5%, and 7% by mass of cement, while the amount of 2-MI curing agent was 50% of the net weight of microcapsules. The detailed mix proportions of the mortar specimens are shown in Table 2. Cement, sand, and 2-MI were first mixed for 2 min, followed by the addition of microcapsules and low-speed mixing for 1 min. Water was then added, and the mixture was stirred at low speed for another 2 min. The fresh mortar was cast into molds of 40 mm × 40 mm × 40 mm, compacted, and covered with a plastic film for 24 h before demolding. The specimens were then cured in a standard curing chamber at 20 ± 3 °C and a relative humidity of ≥ 95% for 28 days.

2.4 Characterization and test approach

2.4.1 Morphology observation

A digital camera and a scanning electron microscope (SEM, TESCAN MIRA) were employed to observe the micro-morphology of the microcapsules and the crack regions. The dried specimens were mounted on conductive adhesive tape and coated with a thin layer of gold to enhance electrical conductivity. SEM images at various magnifications were used to examine the surface features, shell structure, and cross-sectional morphology of the microcapsules, as well as the microstructural characteristics of the mortar specimens at the crack sites.

Table 2 Mix proportion of mortar specimens.

Mortar specimen	Cement (g)	Sand (g)	Water (g)	Microca-psule (g)	2-MI (g)
C0	300	900	150	N/A	N/A
C1	300	900	150	3	1.5
C3	300	900	150	9	4.5
C5	300	900	150	15	7.5
C7	300	900	150	21	10.5

2.4.2 Particle size measurement

Thirty microcapsules were randomly selected from the prepared microcapsules, and their particle sizes were measured and analyzed using the Image J processing software [11]. The average particle size was then calculated based on the statistical results.

2.4.3 Core content measurement

A total of 10 g of microcapsules were randomly selected for the determination of core content. For the microcapsules before soaking in cement filtrate, the specimens were thoroughly ground and crushed, then repeatedly washed three times with acetone and subsequently dried. The mass loss of the microcapsules was taken as the mass of the core material, from which the proportion of core material to the total microcapsule mass was calculated. The cement filtrate was prepared by mixing ordinary Portland cement with deionized water at a water-cement ratio of 1:10 by mass, followed by magnetic stirring at 300 rpm for 2 minutes. The cement filtrate was obtained by vacuum filtration. For the microcapsules after soaking, the core material content was determined using the same procedure.

2.4.4 Thermal stability

Thermogravimetric analysis (TGA) was performed using a Rigaku Thermo Plus EVO2 TG8121 analyzer to evaluate the thermal decomposition behavior of the microcapsules. The specimens were heated from 30 °C to 1000 °C at a rate of 10 °C/min under a nitrogen atmosphere. The mass loss curve was recorded as a function of temperature to analyze the weight loss processes and decomposition mechanisms of the microcapsules within different temperature ranges.

2.4.5 FTIR test

The chemical structure of the prepared microcapsules was characterized using a Fourier transform infrared spectrometer (FTIR, Thermo Fisher Nicolet iS20). The microcapsules were ground and thoroughly mixed with analytical-grade KBr at a mass ratio of approximately 1:100, then pressed into pellets for testing at room temperature. The scanning wavenumber range was set from 4000 to 400 cm^{-1}.

2.4.6 Compressive strength test

The compressive strength of the mortar specimens was tested using a universal testing machine (MTS). After 28 days of curing, the first compressive test was conducted to determine the initial compressive strength. The loading was applied under displacement-controlled mode at a rate of 2.5 kN/s until specimen failure, and the maximum load was recorded to calculate the compressive strength. To evaluate the self-healing performance of the microcapsules, part of the specimens were subjected to controlled crack induction and retesting after the initial test. Each specimen was loaded to approximately 50% of its maximum load capacity to generate controlled microcracks. The cracked specimens were then cured in water for 7 days, during which the microcapsules were activated by crack formation, releasing the epoxy that subsequently underwent self-healing reactions. After the 7-day healing period, a second compressive test was performed, and the maximum load after healing was recorded. The self-healing efficiency (η) was calculated by comparing the compressive strength before and after healing, as defined in Eq. (1):

$$\eta = \frac{f_{healed}}{f_{initial}} \times 100\% \qquad \text{Eq. (1)}$$

where finitial indicates initial compressive strength, fhealed indicates self-healed compressive strength.

2.5 Molecular dynamics simulation

To investigate the curing mechanism of the epoxy core during the self-healing process, MD simulation was conducted to investigate the crosslinking reaction between the epoxy monomer and the curing agent 2-MI [12-14]. The simulation was performed using the Materials Studio software [15]. The epoxy monomer was represented by the diglycidyl ether of bisphenol A (DGEBA) molecule, while 2-methylimidazole (2-MI) was used as the curing agent. The initial model consisted of seven DGEBA molecules and seventy 2-MI molecules, which were randomly mixed under three-dimensional periodic boundary conditions, as illustrated in Fig. 1a. The system then underwent energy minimization and structural optimization to achieve a stable volume fraction and intermolecular interactions, reaching a target density of 1.17 $g \cdot cm^{-3}$. This equilibrated structure served as the initial configuration for subsequent crosslinking and property calculations. In the model, the molecular ratio of DGEBA to 2-MI was set to 1:10. The excess of 2-MI was deliberately chosen to ensure sufficient availability of curing agent molecules to efficiently trigger the epoxy ring-opening reactions and increase the probability of effective crosslinking. The resulting simulation box dimensions were 19.96 Å × 19.96 Å × 19.96 Å.

The Polymer Consistent Force Field (PCFF) force field was employed in this study to perform simulations of the epoxy-imidazole system. The PCFF force field offers good applicability and computational efficiency for simulating polymer crosslinking processes and has been widely recognized as one of the primary force fields for epoxy crosslinking simulations [16, 17]. Since PCFF is an empirical force field rather than a reactive one capable of dynamically forming or breaking bonds, reactive atoms must be pre-defined manually before simulation. In this work, the carbon atoms on the epoxy rings of DGEBA molecules were designated as reactive sites, while the nitrogen atoms in 2-MI molecules were marked as reactive sites, as illustrated in Fig. 1b. Based on the bonding criteria defined in a Perl script, the crosslinking reaction was triggered using a gradually

increasing reaction radius method. Reactive atom pairs were identified, and epoxy ring-opening reactions were performed to generate new bonds and advance the formation of the polymer network.

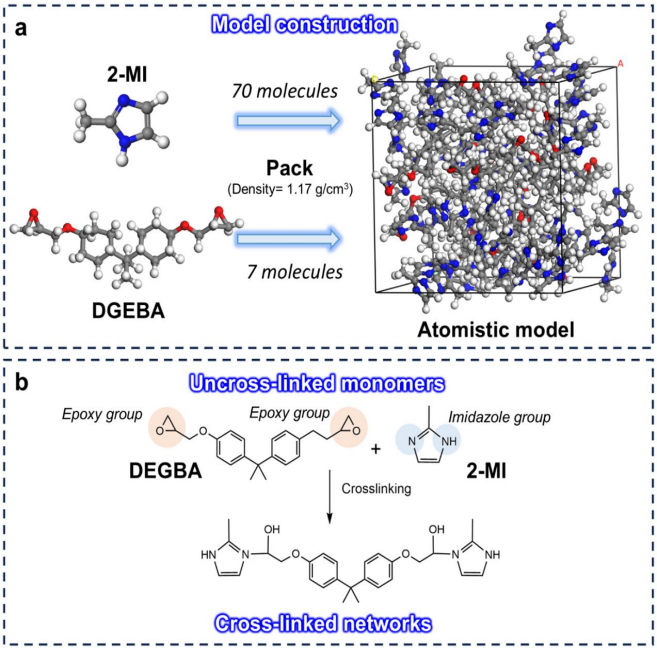

Fig. 1 Atomistic illustration of DGEBA/2-MI material system: (a) Model construction and (b) Reaction sites mark.

The simulation was conducted using a timestep of 1.0 fs, which is typically adopted for polymer systems to ensure energy stability and computational accuracy. Each equilibration stage (NPT at 300 K) was performed for 200 ps prior to bond creation. After each crosslinking iteration, geometry optimization was followed under the NVT ensemble to eliminate local stress. The Perl script then screened for atomic pairs meeting the bonding criteria. For each reactive pair, the epoxy ring in the DGEBA monomer was opened, and a new bond was created between the pair. Subsequently, geometric optimization and relaxation were performed for both the newly bonded regions and the entire system to eliminate local stress and stabilize the structure. The reaction radius was initially set at 2.5 Å and gradually increased to 4.0 Å in increments of 0.5 Å. The lower initial radius helps identify highly probable reaction pairs with strong proximity-driven interaction, while the later extension ensures that all thermodynamically feasible crosslinking sites are captured without artificially forcing bond formation. This procedure was iteratively repeated, with the crosslinking conversion rate calculated after each iteration, until the target conversion was achieved, at which point the crosslinking process was terminated and the final crosslinked structure was output. Throughout the simulation, variations in system energy and crosslinking conversion rate were continuously recorded to capture the dynamic evolution of the epoxy crosslinking process at the atomic scale.

3. Results and discussion

3.1 Fabrication mechanism of microcapsule

The formation of microcapsules is based on the principle of ionic crosslinking. Sodium alginate molecular chains are rich in carboxyl and hydroxyl groups, and when they come into contact with divalent calcium ions (Ca^{2+}), the Ca^{2+} ions replace Na^{+} and coordinate with adjacent carboxylate groups to form a three-dimensional egg-box structure. In this configuration, Ca^{2+} acts as a bridging ion that crosslinks multiple polymer chains, transforming the system rapidly from a solution to a gel network.

During the preparation process, the core material was first dispersed into a sodium alginate solution to form an emulsion, which was then dripped into a $CaCl_2$ solution. As Ca^{2+} diffused into the droplets, gelation initially occurred at the outer layer and gradually proceeded inward as ions penetrated further, resulting in microcapsules with a distinct core-shell structure, as shown in Figs. 2a-b. The compactness and thickness of the shell are jointly influenced by the ion diffusion rate, solution concentration, and stirring conditions: higher Ca^{2+} concentrations or longer contact times lead to greater crosslinking density and denser shells but may also increase brittleness; conversely, lower Ca^{2+} concentrations or shorter crosslinking times yield more flexible shells.

In this study, the concentrations of sodium alginate and calcium chloride solutions were set at 1.5 wt% and 2 wt%, respectively, both within ranges verified as effective in previous publications. When the microcapsules were incorporated into mortar during

mixing and water addition, they exhibited good survivability, as shown in Fig. 2c, where the capsules remained intact, confirming the reliability of the encapsulation process. After 28 days of curing, the embedded microcapsules within the hardened mortar still maintained their intact morphology (Fig. 2d), demonstrating the durability of the encapsulation technique.

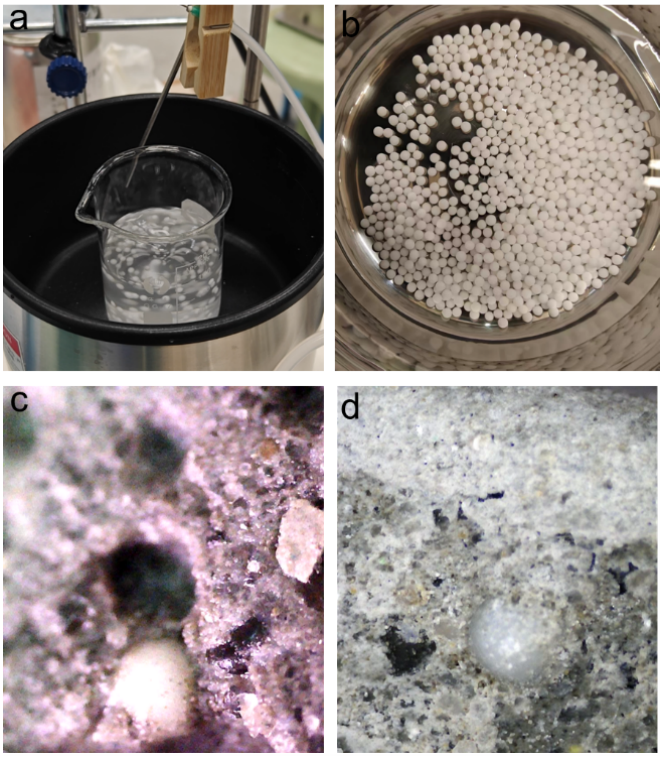

Fig. 2 Electron photographs of the prepared microcapsules and their distribution in mortar: (a) Microcapsules fabricated by the dripping crosslinking method, (b) Prepared microcapsules, (c) Microcapsules embedded in fresh mortar during mixing, and (d) Microcapsules observed in mortar after 28 days of curing.

3.2 Microcapsule morphology

Fig. 3 illustrates the morphological characteristics of the prepared microcapsules. As shown in Fig. 3a, the microcapsules exhibit a regular spherical shape with good dispersion, indicating the successful formation of a stable shell structure during the ionic crosslinking between sodium alginate and calcium chloride. The SEM image in Fig. 3b further reveals that the microcapsules retain their integrity and spherical morphology after drying, without noticeable rupture or collapse, suggesting that the CA network possesses excellent structural stability. A magnified view of the microcapsule surface (Fig. 3c) shows a relatively compact texture with slight wrinkles and fine pores, mainly resulting from water evaporation and alginate shrinkage during the drying process. The moderately rough surface can enhance mechanical interlocking between the microcapsules and the cement matrix, facilitating the triggering of microcapsules upon crack formation. The cross-sectional image of a ruptured microcapsule (Fig. 3d) clearly reveals a porous inner shell structure. These interconnected pores serve as reservoirs for the epoxy core material and provide effective release pathways when cracks occur.

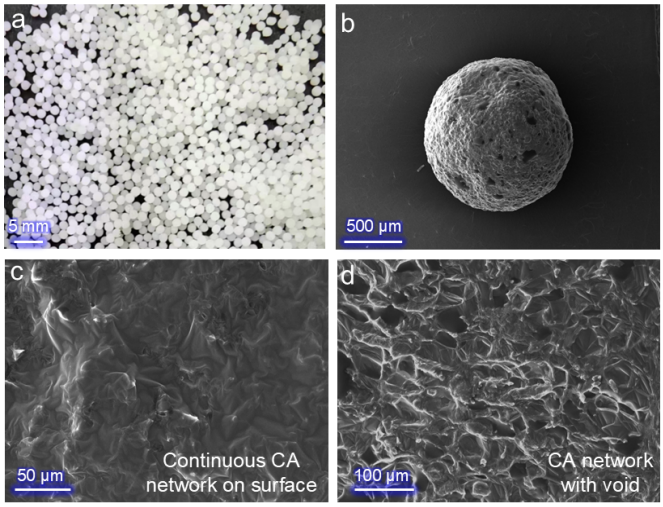

Fig. 3 Morphological characteristics of the fabricated microcapsules: (a) Optical image of dried microcapsules, (b) SEM image of the microcapsules, (c) Magnified view of the microcapsule surface, and (d) Cross-sectional image of a microcapsule.

3.3 Particle distribution of microcapsule

A statistical analysis of the particle size distribution of the prepared microcapsules was conducted. As shown in Fig. 4a, the particle sizes were mainly distributed between 1.50 mm and 1.65 mm, indicating that the droplet formation process during preparation was relatively uniform. The narrow particle size distribution demonstrates that the adopted dripping-ionic crosslinking method enables the stable fabrication of structurally intact microcapsules with controllable

size, providing a solid foundation for their uniform dispersion and effective activation in cementitious materials. The calculated average particle diameter was 1.54 mm, which falls within the typical size range for this preparation technique.

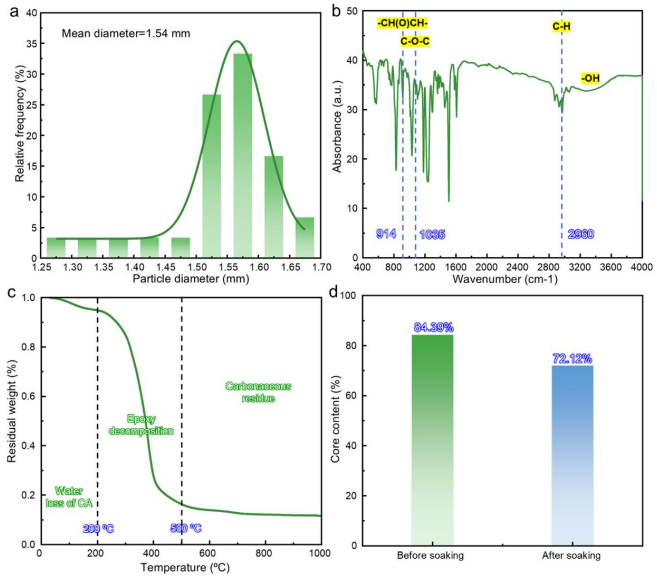

Fig. 4 (a) Particle distribution, (b) FTIR analysis, (c) TG curve, and (d) Core content measurement of microcapsule.

3.4 FTIR analysis

To verify the formation of the CA shell and the successful encapsulation of the epoxy core, FTIR analysis was performed on the prepared microcapsules, and the results are shown in Fig. 4b. For the epoxy core material, a distinct characteristic peak of –CH(O)CH– was observed near 914 cm^{-1}. This peak corresponds to the unreacted epoxy functional groups, indicating that no significant ring-opening or curing reaction occurred during the microcapsule preparation process, thereby confirming the effectiveness of encapsulation. The characteristic peak appearing around 1035 cm^{-1} is attributed to the C-O-C stretching vibrations of both the polysaccharide backbone of CA and the epoxy molecules. The absorption peak near 2960 cm^{-1} corresponds to the C-H stretching vibrations, consistent with the spectroscopic characteristics of E-51 epoxy. Notably, a broad -OH stretching band appears in the range of 3200-3500 cm^{-1}, which can be ascribed to hydrogen-bond interactions between the CA chains and epoxy molecules.

3.5 Thermal stability of microcapsule

Fig. 4c presents the TGA curve of the microcapsules, which was used to evaluate their thermal stability. The thermal decomposition process of the microcapsules can be divided into three main stages.

Initial weight loss stage (approximately 30-200 °C): The mass loss in this stage primarily results from the gradual evaporation of moisture within the shell. CA exhibits strong hydrophilicity, and its crosslinked network contains abundant carboxylate and hydroxyl groups capable of forming hydrogen bonds with water molecules. Consequently, a noticeable yet slow weight loss is observed within this temperature range.

Major decomposition stage (approximately 200-500 °C): This stage corresponds to the principal pyrolysis process of the microcapsules, involving both the degradation of the CA shell and the volatilization of part of the core material. The glycosidic and carboxylate bonds within the shell begin to break, releasing CO^2 and small molecular fragments. Simultaneously, the epoxy core undergoes gradual thermal decomposition, resulting in the maximum weight-loss peak.

Residual stage (above 500 °C): At higher temperatures, the weight loss tends to stabilize, with the residual mass accounting for approximately 10-20% of the initial mass. This residue mainly consists of carbonaceous and organic remnants.

3.6 Core content of microcapsule

Fig. 4d shows the change in core content of the microcapsules before and after immersion in cement filtrate, which was used to evaluate their core retention performance under alkaline conditions. As shown in the figure, the core content of the microcapsules before immersion was 84.39%, indicating that the epoxy was effectively encapsulated within the CA shell during preparation, forming a dense and structurally intact core–shell system. After immersion in cement filtrate for 1 day, the core content decreased to 72.12%, suggesting a slight leakage of the core material in the alkaline environment. This minor loss is mainly attributed to the swelling of the CA shell under alkaline

conditions, which enlarges the pore size of the shell and facilitates limited diffusion of the encapsulated epoxy.

Nevertheless, the microcapsules retained over 70% of their core content after immersion, demonstrating excellent chemical stability and core retention capability. These results confirm that the Ca^{2+}-crosslinked alginate shell maintains good structural integrity in highly alkaline environments, ensuring sufficient availability of the epoxy for subsequent release and self-healing reactions upon crack activation.

3.7 Compressive strength of mortar

Fig. 5 presents the variations in compressive strength and self-healing efficiency of mortar specimens containing different microcapsule dosages (0, 1, 3, 5, and 7 wt%) before and after healing. The results indicate that the incorporation of microcapsules has a significant influence on both the initial strength and the healing performance of the mortar. With increasing microcapsule content, the initial compressive strength decreased gradually from 36.10 MPa for the control group (C0) to 20.19 MPa for the C7 group. At low dosages (1-3 wt%), the strength slightly decreased (33.24 MPa and 30.08 MPa, respectively), primarily due to the formation of localized weak interfaces between the microcapsules and the cement matrix. However, when the dosage was further increased to 5 wt% and 7 wt%, the strength reduction became more pronounced (decreasing by approximately 25.9% and 44.0%, respectively), which can be attributed to the excessive introduction of voids caused by surplus microcapsules.

After crack healing, all specimens exhibited varying degrees of strength recovery. The control group (C0) showed a post-healing strength of 36.66 MPa, indicating negligible self-healing efficiency (101.55%), as expected. In contrast, the specimens containing microcapsules demonstrated remarkable improvement: the C3 and C5 groups exhibited healed strengths of 36.21 MPa and 38.88 MPa, corresponding to self-healing efficiencies of 120.38% and 145.40%, respectively. Notably, the C5 group achieved a strength increase of approximately 45% compared with its initial value, suggesting that a 5 wt% dosage provided sufficient epoxy release upon crack activation, leading to the formation of dense crosslinked healing products. However, further increasing the dosage to 7 wt% resulted in a healed strength of only 19.63 MPa (self-healing efficiency 97.23%), indicating that excessive microcapsules disrupt matrix continuity and compromise overall healing performance.

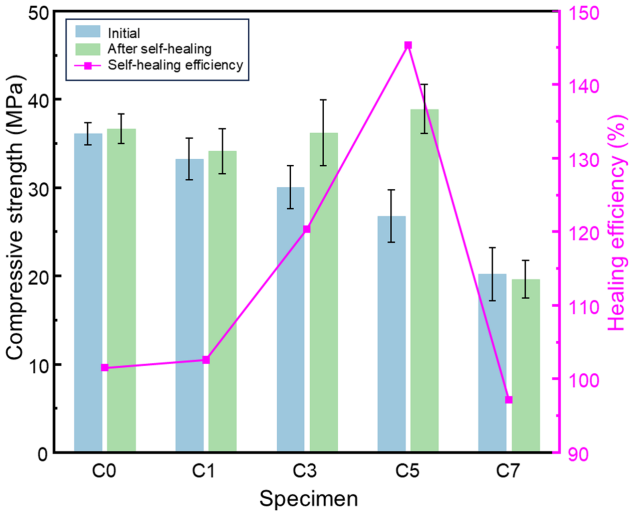

Fig. 5 Compressive strength and self-healing efficiency of mortar specimens with different microcapsule dosages before and after healing.

3.8 Self–healing product

Fig. 6 illustrates the morphological evolution of the self-healing process of microcapsules at the crack regions in mortar. As shown in Fig. 6a, the microcapsules are uniformly distributed within the hardened mortar and tightly bonded to the surrounding matrix, indicating good structural stability during mixing and curing. When cracks form in the mortar, some microcapsules rupture due to localized stress concentration, releasing the epoxy core material that subsequently infiltrates the crack region (Fig. 6b). The clearly visible fractured interfaces and the flow of the epoxy phase confirm that the microcapsules can be effectively activated under external stress, achieving stress-responsive release. In the cracked region, the released epoxy rapidly fills and cures within the crack, forming dense repair products (Fig. 6c). The solidified epoxy adheres to the cement matrix, effectively sealing

the crack and preventing the ingress of moisture and ions from the external environment. At higher magnification (Fig. 6d), a well-bonded interface between the cured epoxy and the cement hydration products can be observed, where the epoxy adheres intimately to the hydrated phases. This interfacial bonding results in the formation of a continuous and compact layer along the crack, thereby restoring the structural integrity and mechanical performance of the mortar matrix.

It should be noted that although the epoxy-based microcapsules demonstrated satisfactory crack healing and strength recovery in laboratory conditions, the potential degradation of epoxy under real crack environments, for example, long-term degradation as well as possible debonding at the epoxy-cement interface under aggressive exposure scenarios, are not evaluated in this study. These aspects may affect the long-term repair effectiveness and should be further investigated in future work to assess the durability of the self-healing system under realistic service conditions.

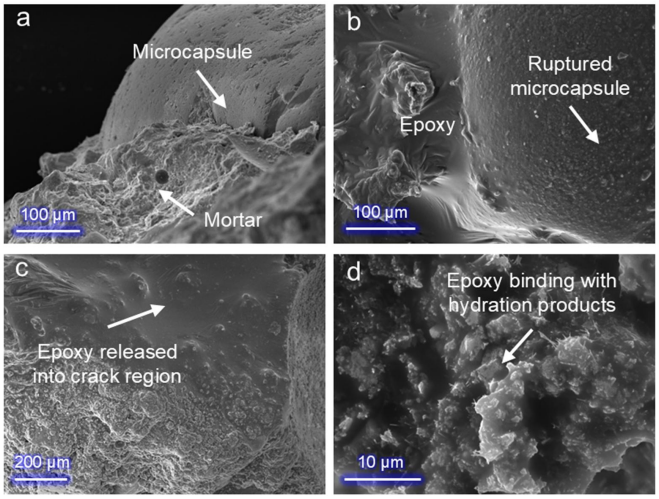

Fig. 6 SEM images showing the self-healing process of microcapsules: (a) Microcapsules embedded in the mortar matrix, (b) Ruptured microcapsules releasing epoxy under crack-induced stress, (c) Cured epoxy products filling the crack region, (d) Interfacial bonding between the cured epoxy and hydration products.

3.9 Molecular self–healing process

To elucidate the molecular mechanism of the microcapsule core during crack repair, an atomistic simulation was performed to investigate the crosslinking reaction between the epoxy core (DGEBA molecule) and the curing agent (2-MI molecule). Since the simulation triggered new chemical bond formation by gradually increasing the reaction radius, the evolution of system temperature, potential energy, and crosslinked structure was analyzed as a function of reaction radius.

As shown in Fig. 7a, when the reaction radius increased from 2.5 Å to 4.0 Å, the average system temperature slightly decreased from 291.81 K to 289.34 K, indicating that bond formation occurred under nearly isothermal conditions. In contrast, the potential energy of the system dropped significantly from -2555.55 kcal/mol to -3457.54 kcal/mol, with a total reduction of 902 kcal/mol, demonstrating that as the reaction radius expanded, more reactive atoms were included within the bonding region, promoting chemical bond formation and leading to a more stable configuration. Notably, a sharp decrease in potential energy occurred at a reaction radius of approximately 3.5 Å, marking the key stage of rapid crosslink network formation. Fig. 7b shows the variation in crosslinking conversion and average bond energy with reaction radius. As the reaction radius increased, the conversion rate gradually rose from 7.14% to 92.86%, indicating that the reaction between epoxy groups and imidazole molecules evolved from local bonding in the initial stage to an almost fully crosslinked three-dimensional network. Meanwhile, the average bond energy increased from 559.50 kcal/mol to 585.04 kcal/mol, followed by a slight decrease to 556.45 kcal/mol. This initial increase and subsequent decline suggest that C-N bonds predominantly formed during the early reaction stage, while structural relaxation in the later stage led to a more stable chemical configuration.

From a structural perspective, Fig. 7c depicts the uncross-linked model, where the molecular chains are loosely arranged with visible intermolecular voids. As the reaction proceeded (Fig. 7d), a continuous and compact three-dimensional crosslinked network was formed, with significantly reduced intermolecular distances and enhanced structural density. The locally magnified view (Fig. 7e) clearly reveals typical C-N

bond formation, confirming the active crosslinking sites between DGEBA and 2-MI. This microscopic bonding process corresponds to the macroscopic curing and strength recovery behavior of the epoxy core observed in the self-healing experiments.

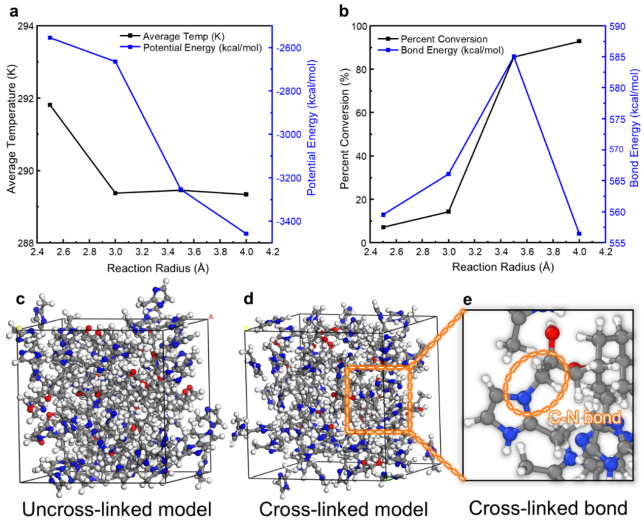

Fig. 7 Molecular responses of DGEBA/2-MI system: (a) Average temperature and potential energy varied with reaction radius, (b) Percent conversion rate and bond energy varied with reaction radius, (c) Uncross-linked model morphology, (d) Crosslinked model morphology, and (e) Formed C-N bond between DGEBA and 2-MI.

The simulation revealed the progressive formation of new covalent bonds between DGEBA and 2-MI molecules, indicating the development of a stable crosslinked polymer network during curing. This simulated network formation is consistent with the experimentally observed healing behavior, where the released epoxy effectively sealed the cracks and contributed to strength recovery. The molecular-scale densification effect predicted in the simulation aligns with the macroscopic consolidation of the crack area observed after healing, suggesting that the formation of a highly crosslinked epoxy structure at the crack interface is the primary mechanism driving the performance enhancement. These findings indicate that the simulation results provide mechanistic evidence supporting the experimental healing efficiency and confirm the feasibility of embedding epoxy-based microcapsules for autonomous self-repair in cementitious materials.

The MD model focused exclusively on the interactions between epoxy and the curing agent, without considering the complex physicochemical environment at the crack interface in concrete. Factors such as the presence of hydration products and moisture transport effects were not included. These environmental interactions may influence epoxy curing behavior and interfacial bonding performance and should therefore be examined in future studies through multi-scale simulation combined with experimental validation.

Conclusions

(1) The fabricated microcapsules exhibit excellent thermal stability within the temperature range of 30-200 °C, showing no significant structural decomposition. This indicates that the microcapsules can withstand the typical temperature conditions encountered during the cement hydration process.

(2) Both macroscopic and microscopic observations confirm that the CA shell successfully encapsulated the epoxy core, forming well-defined and structurally stable microcapsules suitable for self-healing applications in cementitious materials.

(3) The incorporation of microcapsules can significantly enhance the mechanical recovery of mortar after cracking. Insufficient epoxy release occurs at low dosages, while excessive dosages lead to increased porosity and a reduction in initial strength. Considering both compressive strength and self-healing efficiency, a 5 wt% microcapsule dosage was identified as the optimal content, at which the system achieves a balance between structural integrity and high healing efficiency, providing experimental evidence for realizing effective self-healing performance.

(4) The MD simulation revealed the atomic-level mechanism underlying the curing behavior of the epoxy core during the self-healing process. The gradual

formation of C-N bonds between DGEBA and 2-MI molecules and the evolution toward a dense three-dimensional crosslinked network correspond well with the experimental observations of crack filling and strength recovery. This consistency between simulation and experimental results provides a molecular-level interpretation of the macroscopic self-healing behavior.

Acknowledgements

The work described in this paper was supported by a grant from the Research Grants Council of the Hong Kong Special Administrative Region, China (Project No. CityU R1018-22).

Reference

[1] Micaelo, R., T. Al-Mansoori, and A. Garcia, Study of the mechanical properties and self-healing ability of asphalt mixture containing calcium-alginate capsules. Construction and Building Materials, 2016. 123: p. 734-744.

[2] Zhang, L., et al., Synthesis and characterization of multi-cavity Ca-alginate capsules used for self-healing in asphalt mixtures. Construction and Building Materials, 2019. 211: p. 298-307.

[3] Cui, K., et al., Investigation of the macro performance, mechanism, and durability of multiscale steel fiber reinforced low-carbon ecological UHPC. Construction and Building Materials, 2022. 327: p. 126921.

[4] Cui, K., et al., Mechanical properties and mechanism of nano-CaCO3 enhanced sulphoaluminate cement-based reactive powder concrete. Construction and Building Materials, 2021. 309: p. 125099.

[5] Cui, K., et al., Understanding the role of carbon nanotubes in low carbon sulfoaluminate cement-based composite. Journal of Cleaner Production, 2023. 416: p. 137843.

[6] Wang, P., et al., Enhanced self-healing performance of cementitious materials using nano-SiO2 modified ethyl cellulose microcapsules. Construction and Building Materials, 2025. 458: p. 139555.

[7] Wang, X., et al., Laboratory and field study on the performance of microcapsule-based self-healing concrete in tunnel engineering. Construction and Building Materials, 2019. 220: p. 90-101.

[8] Dong, S., et al., Robust poly (urea-formaldehyde)/sodium alginate microcapsules for achieving efficient self-healing in concrete. Colloids and Surfaces A: Physicochemical and Engineering Aspects, 2025. 717: p. 136760.

[9] Huang, Y., et al., Dynamic behavior of microcapsule-based self-healing concrete subjected to impact loading. Construction and Building Materials, 2021. 301: p. 124322.

[10] Ying, Y., et al., Self-healing in cementitious system using interface enhanced capsules prepared at room temperature. Journal of Cleaner Production, 2023. 395: p. 136465.

[11] Abràmoff, M.D., P.J. Magalhães, and S.J. Ram, Image processing with ImageJ. Biophotonics international, 2004. 11(7): p. 36-42.

[12] Zhao, D., et al., Tailored twisted CNT bundle with improved inter-tube slipping performances. Thin-Walled Structures, 2024. 196: p. 111536.

[13] Wu, R., et al., Degradation of fiber/matrix interface under various environmental and loading conditions: Insights from molecular simulations. Construction and Building Materials, 2023. 390: p. 131101.

[14] Hou, J.-a., et al. Machine learning-based investigations on nonlinear vibrations of CFRP composite. in 11th International Conference on Fiber-Reinforced Polymer (FRP) Composites in Civil Engineering (CICE 2023). 2023. Zenodo.

[15] Accelrys, I., Materials studio accelrys software inc. San Diego, 2010.

[16] Tam, L.-h., et al., Understanding the effect of temperature on the interfacial behavior of

CFRP-wood composite via molecular dynamics simulations. Composites Part B: Engineering, 2017. 109: p. 227-237.
[17] Tam, L.-h., et al., Effect of hygrothermal environment on traction-separation behavior of carbon fiber/epoxy interface. Construction and Building Materials, 2019. 220: p. 728-738.